

Article

Chemical Instability-Induced Wettability Patterns on Superhydrophobic Surfaces

Tianchen Chen ^{1,2} and Faze Chen ^{1,*} ¹ School of Mechanical Engineering, Tianjin University, Tianjin 300350, China; chentianchen@tute.edu.cn² Laboratory of Packaging Engineering and Visual Interaction Design, Tianjin University of Technology and Education, Tianjin 300222, China

* Correspondence: faze.chen@tju.edu.cn

Abstract: Chemical instability of liquid-repellent surfaces is one of the nontrivial hurdles that hinders their real-world applications. Although much effort has been made to prepare chemically durable liquid-repellent surfaces, little attention has been paid to exploit the instability for versatile use. Herein, we propose to create hydrophilic patterns on a superhydrophobic surface by taking advantage of its chemical instability induced by acid solution treatment. A superhydrophobic Cu(OH)₂ nanoneedle-covered Cu plate that shows poor stability towards HCl solution (1.0 M) is taken as an example. The results show that 2.5 min of HCl solution exposure leads to the etching of Cu(OH)₂ nanoneedles and the partial removal of the self-assembled fluoroalkyl silane molecular layer, resulting in the wettability transition from superhydrophobicity to hydrophilicity, and the water contact angle decreases from ~160° to ~30°. Hydrophilic dimples with different diameters are then created on the superhydrophobic surfaces by depositing HCl droplets with different volumes. Afterwards, the hydrophilic dimple-patterned superhydrophobic surfaces are used for water droplet manipulations, including controlled transfer, merging, and nanoliter droplet deposition. The results thereby verify the feasibility of creating wettability patterns on superhydrophobic surfaces by using their chemical instability towards corrosive solutions, which broadens the fabrication methods and applications of functional liquid-repellent surfaces.

Keywords: superhydrophobic surface; chemical instability; wettability pattern; droplet manipulation



Citation: Chen, T.; Chen, F. Chemical Instability-Induced Wettability Patterns on Superhydrophobic Surfaces. *Micromachines* **2024**, *15*, 329. <https://doi.org/10.3390/mi15030329>

Academic Editor: Hongjie An

Received: 18 January 2024

Revised: 21 February 2024

Accepted: 25 February 2024

Published: 27 February 2024



Copyright: © 2024 by the authors. Licensee MDPI, Basel, Switzerland. This article is an open access article distributed under the terms and conditions of the Creative Commons Attribution (CC BY) license (<https://creativecommons.org/licenses/by/4.0/>).

1. Introduction

Bio-mimic superhydrophobic surfaces have drawn rapidly increasing research interest because of their great significance for versatile applications such as self-cleaning [1,2], chemical detection and sensors [3–6], liquid droplet/gas bubble manipulation [7–11], icephobicity [12–16], immiscible liquid separation [17–19], enhanced heat transfer [20–22], and anti-corrosion [23–25]. However, most superhydrophobic surfaces suffer from chemical instability in harsh conditions like highly concentrated acidic/alkaline/salty solution immersion, organic solvent invasion, thermal treatment, UV irradiation, and active species exposure [26–28]. The chemical instability usually results in the loss of superhydrophobicity to varying degrees due to interfacial chemical process-induced surface chemistry and/or morphology change, which could obviously shorten the lifespan of superhydrophobic surfaces and thus be commonly considered one of the major limitations for their real-world applications. As a result, great efforts have been made to fabricate chemically durable superhydrophobic surfaces, and much progress has been achieved in recent years [27,28].

Although chemically stable superhydrophobic surfaces are crucial in some cases, such as chemical shielding and anti-corrosion [29–31], external stimuluses triggered chemical instabilities are sometimes more desired, especially in the construction of functional surfaces with (super)hydrophilic–superhydrophobic patterns or reversible wettability [28,32–34]. Surfaces with extreme wettability patterns are widely used in various applications such

as enhanced water harvesting, spontaneous liquid transport, etc. [28,35]. For example, Bai et al. [36] took the advantage of the chemical instability of superhydrophobic TiO₂ coatings upon UV exposure to prepare star-shaped superhydrophilic patterns on superhydrophobic surfaces, which were used to realize efficient water harvesting by integrating the water collection strategies of both desert beetles and spider silk. By using a similar patterning method, Ghosh et al. [37] prepared wedge-shaped superhydrophilic patterns on superhydrophobic TiO₂ surfaces and realized high-rate, pumpless liquid transport on the open substrates. Xu et al. [38] reported selective UV irradiation-induced superhydrophilic patterns on an octadecyltrichlorosilane-modified superhydrophobic silica coating and demonstrated its potential application towards microgravity biosensing. Plasma contains active species, such as high-energy electrons, metastable particles, etc., so it can always initiate surface chemistry and/or texture changes and thus, cause instability (i.e., hydrophilization) of superhydrophobic surfaces [32]. For example, Huang et al. [39] used the chemical instability of a superhydrophobic surface towards plasma treatment to fabricate superhydrophilic patterns on the superhydrophobic surface, which was further used for underwater spontaneous pumpless transportation of organic liquids. Liu et al. [40] fabricated hydrophilic patterns on a superhydrophobic surface by micro-plasma jet treatment and reported its versatile ability to control water adhesion. Additionally, Liu et al. [41] showed that a superhydrophobic Cu mesh could be completely converted to be superhydrophilic after being immersed in tetrahydrofuran for 5 min, which facilitated subsequent reversible oil/water separation. Therefore, the chemical instability of superhydrophobic surfaces towards external stimuluses is not always a drawback for their applications; making ingenious use of the instability can provide additional possibilities for constructing special functional surfaces [28].

Immersion in an acidic/alkaline/salty solution, triggering chemical corrosion, can sometimes change the surface morphology and/or surface chemistry of superhydrophobic surfaces, thereby changing their surface wettability (i.e., chemical instability) [42–45]. Although some works involving pH-responsive switchable super-wettability have been reported [43–45], they were limited to smart surface fabrication or reversible oil/water separation, indicating that the full exploitation of their chemical instability for beneficial usage was largely insufficient. In this paper, we took a superhydrophobic Cu(OH)₂ nanorod-covered Cu surface, which was unstable towards HCl solution exposure, as an example to demonstrate the feasibility of creating wettability patterns by using this chemical instability. Chemical etching by an HCl solution (1.0 M, 2.5 min) turned the superhydrophobic surface into a hydrophilic one, and the related mechanism of the wettability transition was studied. Hydrophilic dimple-patterned superhydrophobic surfaces were then prepared and employed to realize water droplet manipulation, such as transfer, merging, and deposition.

2. Materials and Methods

Copper plates (3 × 4 × 0.1 cm³) were bought from Huaru copper Co., Ltd. (Guangzhou, China). Analytical-grade ethanol, HCl, NaOH, and (NH₄)₂S₂O₈ were supplied by Tianjin Kemiou Chemical Reagent Co., Ltd. (Tianjin, China). 1H,1H,2H,2H-Perfluorodecyltriethoxysilane (fluoroalkyl silane, FAS) with 97% purity was purchased from Alfa Aesar (Haverhill, MA, USA).

A superhydrophobic surface on a copper substrate was fabricated according to a previously reported method [46]. Briefly, a copper plate was firstly polished mechanically using 1000# and 2000# abrasive paper and then ultrasonically cleaned in sequence in HCl (0.1 M), alcohol, and deionized water. Then, the cleaned copper plate was placed into an aqueous solution containing NaOH (2.5 M) and (NH₄)₂S₂O₈ (0.1 M) for 5 min to construct micro/nano structures. Then, the substrate was taken out and washed with abundant ultrapure water. After drying with blowing air, the sample was immersed into 1 wt% ethanol solution of FAS for 1 h to lower the surface energy. Then, the plate was washed with ethanol and dried at 90 °C. Finally, the copper surface was imparted with superhydrophobicity.

The instability of the obtained superhydrophobic Cu surface was triggered by an HCl (1.0 M) solution, and the chemical instability was characterized by the water contact angles (WCAs) of the surface after being exposed to the HCl solution for different times (0–5 min). Hydrophilic dimple patterns were fabricated by depositing HCl (1.0 M) droplets with different volumes (0.2–5.0 μL) on the as-prepared superhydrophobic Cu surfaces for 2.5 min. After reaching the specific reaction time, the residual liquid was removed by absorbent paper, and the surfaces were washed with deionized water and then blow-dried at room temperature.

The WCAs of the sample surfaces were measured by an optical contact angle meter (AST-VCM Optima, Billerica, MA, USA) at room temperature. The 3D morphology and corresponding cross-sectional profile were recorded by a confocal laser scanning microscope (CLSM, Carl Zeiss LSM 700, Jena, Germany). The surface morphologies and corresponding chemical compositions of the samples were observed by scanning electron microscope (SEM, SUPRA 55 SAPPHIRE, Oberkochen, Germany) at an accelerating voltage of 15 kV. The surface chemical groups were analyzed by Fourier transform infrared spectrophotometer (FTIR, JASCO, Tokyo, Japan). The surface chemistries were also characterized by X-ray photoelectron spectroscopy (XPS, Thermo ESCALAB 250Xi, Waltham, MA, USA) with a monochromatic Al K α (1486.6 eV) X-ray beam, and the C 1s peak at 284.8 eV was used as reference. The spot size was 400 μm , and the pass energy and energy step size of the full spectrum scan were, respectively, 100 eV and 1.0 eV, while those of the C 1s high-resolution spectrum were 50.0 eV and 0.1 eV, respectively. An X-ray diffractometer (XRD, Bruker AXS D8 Discover, Bremen, Germany) with an X-ray source of Cu K α ($\lambda = 1.5418 \text{ \AA}$) was used to observe the crystal-phase structure of the samples; the scanning rate was $2^\circ / \text{min}$.

3. Results and Discussion

The as-prepared superhydrophobic Cu surface possessed excellent water repellence with a water contact angle (WCA) of 160° , and the solid–liquid interfacial adhesion was negligible when it was pressed to make contact with a water droplet (5.0 μL), as shown in Figure 1a. By contrast, as illustrated in Figure 1b, if the superhydrophobic substrate was moved up and contacted an HCl droplet (1.0 M, 5.0 μL), obvious interfacial adhesion could be observed when the substrate was moved down, and the HCl droplet was even dragged down from the liquid-feeding outlet and then tightly adhered on the surface, demonstrating locally damaged water repellence of the surface upon HCl droplet exposure. The HCl solution-induced chemical instability of the superhydrophobic surface was further studied by measuring the WCA of samples that were immersed in HCl for different durations. Figure 1c shows the influence of immersion time on the WCA of the superhydrophobic surface. It can be seen that the WCA decreased with the immersion time in HCl, and the surface lost its superhydrophobicity after several seconds of chemical etching. Finally, the WCA stabilized at $\sim 30^\circ$ after immersion for 150 s, the surface turned its color to bronze, and the deposited water droplet spread rather than beaded up on the etched surface, as depicted in Figure 1d, indicating complete loss of the water repellence by exposing the surface to the corrosive HCl solution.

Taking advantage of the HCl-induced chemical instability of the superhydrophobic surfaces, hydrophilic patterns can be constructed on the surfaces. Here, we propose to create hydrophilic dimple patterns on superhydrophobic Cu surfaces by depositing HCl droplets on the surface to trigger localized chemical etching, as illustrated in Figure 2a. Figure 2b–f show the surface morphology characterizations of the dimple pattern prepared by using a HCl droplet with volume of 0.2 μL . As depicted in Figure 2b,c, the CSML image and the corresponding cross-sectional profile clearly showed that a circular dimple with diameter of $\sim 390 \mu\text{m}$ and depth of $\sim 3 \mu\text{m}$ was obtained on the superhydrophobic surface. It is widely known that when a water droplet is deposited on a superhydrophobic surface, a circular liquid–solid–vapor composite contacting the interface can be built. Here, the placed HCl droplet-triggered chemical corrosion occurred at the HCl-Cu(OH) $_2$ contact area and finally created a dimple pattern with a round shape. Figure 2d–f show

SEM images of the hydrophilic dimple-patterned superhydrophobic surface with different magnifications. It can be clearly seen that the as-prepared superhydrophobic Cu surface (i.e., the unetched area in Figure 2d) was covered with numerous nanorods and some flower-like microstructures, as can be observed in Figure 2e. By contrast, after being etched by an HCl droplet, the nanorods and flower-like microstructures were obviously destroyed and replaced by closely packed irregular particles with sizes in a range from hundreds of nanometers to several micrometers (Figure 2f). Zooming into these irregular particles revealed that they were decorated with nano-scale granules.

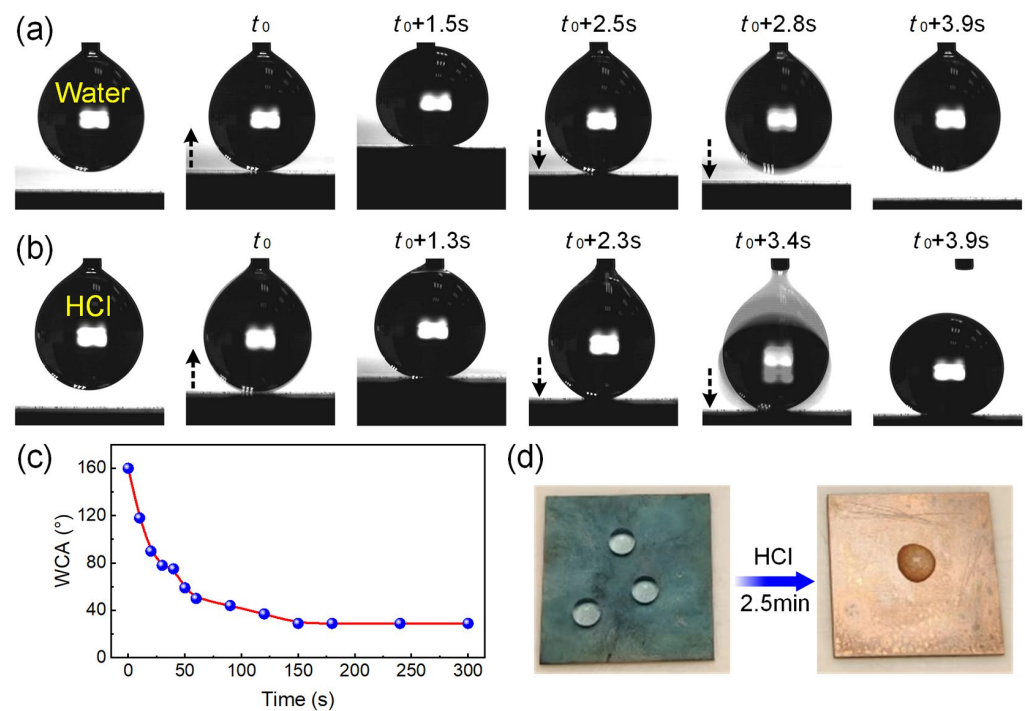


Figure 1. Chemical instability of the superhydrophobic Cu substrate towards HCl solution: image sequences showing the dynamic processes of (a) a water droplet (5.0 μL) and (b) an HCl droplet (1.0 M, 5.0 μL) contacting and detaches from the superhydrophobic surfaces, the arrows indicate the moving directions of the superhydrophobic surfaces; (c) the influence of immersion time in HCl solution on the WCA of the superhydrophobic surface; (d) digital image of water droplets on the original and HCl-etched (for 2.5 min) superhydrophobic surface.

Figure 3 shows the surface chemistries of the original and HCl-etched areas on the superhydrophobic Cu surface. Figure 3a shows the FTIR spectra of the two areas, and the bands around 1139, 1211, and 1241 cm^{-1} were attributed to the $-\text{CF}_2$ and $-\text{CF}_3$ groups [47]. The weak bands at 779 cm^{-1} were assigned to the $\text{Si}-\text{O}-\text{CH}_2\text{CH}_3$ groups of the FAS molecules [48], while the emergence of peaks around 894 cm^{-1} were related to the stretching vibrations of the $\text{Si}-\text{O}-\text{Si}$ bonds [47]. The $\text{Si}-\text{O}-\text{CH}_2\text{CH}_3$ groups in the FAS molecule were transformed into $\text{Si}-\text{OH}$ groups due to the hydrolysis reaction in ethanol solution [49,50]. When the rough Cu substrate was immersed in the ethanol solution of FAS, a second hydrolysis reaction between the $\text{Si}-\text{OH}$ groups and the surface $-\text{OH}$ groups occurred to form $\text{Si}-\text{O}-\text{Cu}$ bonds, which enabled successful self-assembly of the FAS molecules on the Cu surface. Some adjacent self-assembled FAS molecules underwent further dehydration and condensation reactions to form $\text{Si}-\text{O}-\text{Si}$ bonds, leading to the formation of a denser fluorosilane network to impart the rough Cu surface with superhydrophobicity [48,49]. It can be observed that after HCl etching, the intensities of these peaks decreased, especially those originating from the FAS molecules, indicating that the self-assembled FAS coating was partially removed.

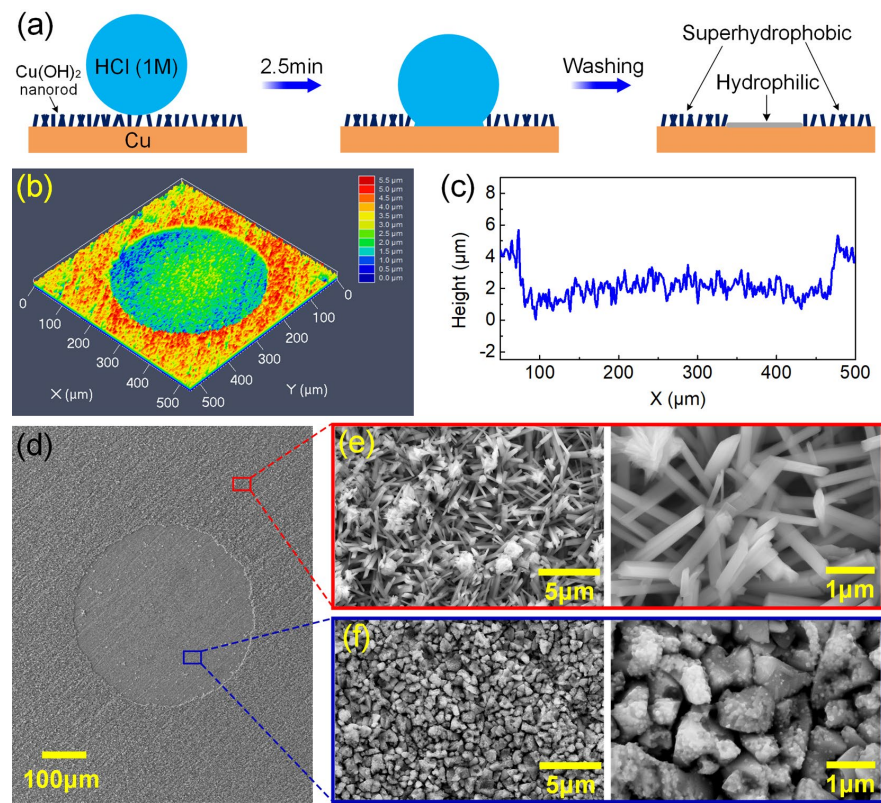


Figure 2. Surface morphologies of the HCl droplet (0.2 μL)-etched superhydrophobic surface: (a) the CLSM image and (b) the corresponding cross-sectional profile; (c–f) SEM images with different magnifications.

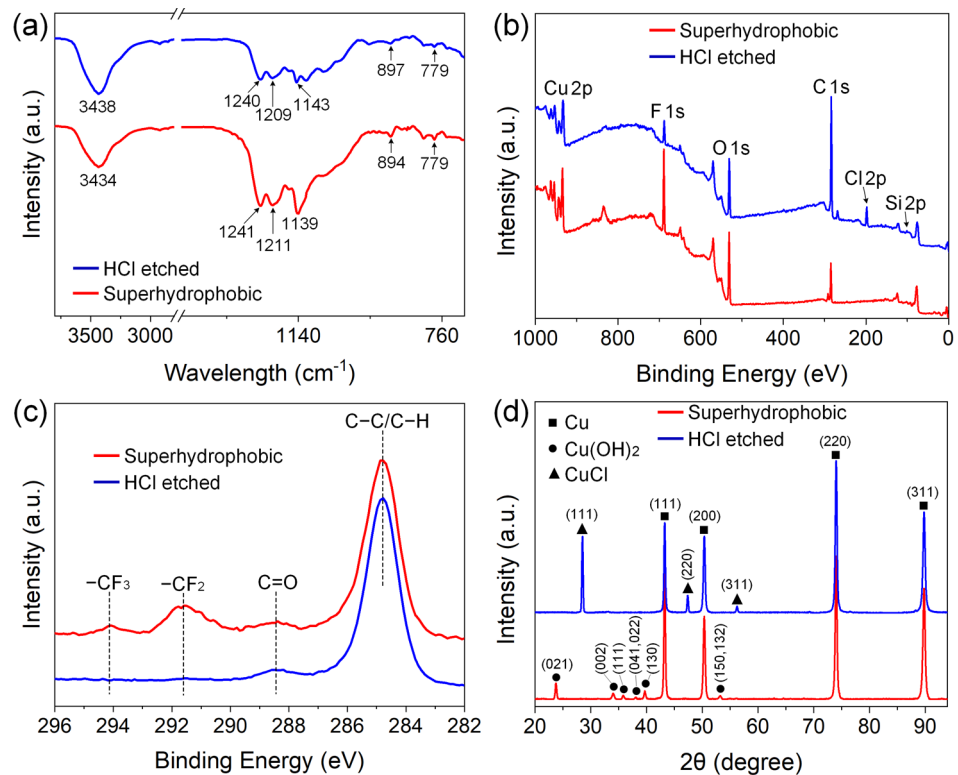
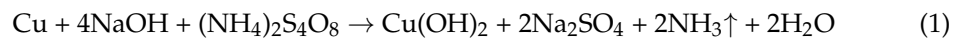
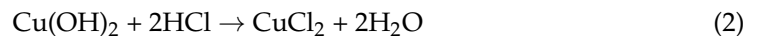


Figure 3. Surface chemistries of the original and HCl-etched areas on superhydrophobic Cu surface: (a) FTIR spectra; (b) XPS spectra; (c) high-resolution C 1s spectra; (d) XRD patterns.

Figure 3b depicts the XPS spectra of the superhydrophobic and HCl-etched areas, and elements of Cu, C, O, F, and Si could be detected. The relative atomic percent of element F was measured to be 20.8% at the original superhydrophobic area, which originates from FAS molecules and contributes to the formation of superhydrophobicity. After HCl etching, the surface F decreased to 4.17%, Cu reduced from 14.74% to 7.61%, and O decreased from 26.74% to 15.78%. Notably, Cl with a content of 4.97% was detected in the HCl-etched area. According to the high-resolution C 1s spectra shown in Figure 3c, the peaks assigned to the $-\text{CF}_2$ and $-\text{CF}_3$ groups of the FAS molecules were markedly detected on the superhydrophobic area [31], while the corresponding peaks for the HCl-etched area could hardly be observed; that is, the peak intensities were greatly weakened after HCl-induced corrosion. Figure 3d shows the XRD patterns of the original superhydrophobic area and HCl-etched area. It can be seen that, besides the diffraction peaks at $2\theta = 43.3$, 50.4 , 74.1 , and 89.9° , respectively attributed to face-centered cubic Cu planes of (111), (200), (220), and (311) (JCPDS card No. 04-0836) that originated from the Cu substrate, new orthorhombic-phase $\text{Cu}(\text{OH})_2$ planes of (021) at 23.7° , (002) at 34.0° , (111) at 35.8° , (041, 022) at 38.0° , (130) and 39.7° , and (150, 132) at 53.2° (JCPDS card No. 80-0656) were detected, confirming the well-known alkali-assisted oxidation of Cu to generate $\text{Cu}(\text{OH})_2$ [46,51]:



In comparison, these diffraction peaks of $\text{Cu}(\text{OH})_2$ disappeared after HCl etching, while three new characteristic peaks corresponding to CuCl planes of (111) at 28.6° , (220) at 47.5° , and (311) at 56.3° (JCPDS card No. 06-0344) were observed. It is commonly known that neutralization happens when $\text{Cu}(\text{OH})_2$ contacts HCl, as described in the following equation:



Then, the generated CuCl_2 could partly etch the exposed Cu substrate with the assistance of HCl, which was finally reduced to CuCl and precipitated on the Cu substrate [52,53]:



According to the above results, we could conclude that NaOH-assisted surface oxidation generated $\text{Cu}(\text{OH})_2$ micro/nano rough structures on the Cu substrate, and the subsequent immersion in FAS successfully triggered the formation of an F-containing monolayer with low surface tension; the obtained surface thereafter possessed superhydrophobicity [46,54]. However, when HCl solution invaded, the $\text{Cu}(\text{OH})_2$ nanorods were chemically etched and partially washed away, as well as the self-assembled FAS layer, which resulted in the content decrease in surface Cu, O, and F. Therefore, the HCl-etched area lost its superhydrophobicity and showed hydrophobicity, which enabled us to construct hydrophobic patterns on the superhydrophobic Cu surface by using its chemical instability towards HCl.

We then examined the influence of the volume of the deposited HCl droplet (V_{HCl} , 0.2–5.0 μL) on the diameter of the obtained dimple (D); the results are depicted and fitted in Figure 4. It can be seen that the diameter of the obtained dimple grew almost linearly with the increase in V_{HCl} . For example, when the V_{HCl} was as small as 0.2 μL , a dimple with a diameter of 0.38 ± 0.02 mm could be obtained. Smaller HCl droplets could hardly generate observable dimples due to their rapid evaporation. When the V_{HCl} was increased to 1.0 μL , the dimple diameter was about 0.47 ± 0.01 mm, and it increased to 0.91 ± 0.03 mm when the V_{HCl} was 5.0 μL . According to the linear fitting of the experimental data (the correlation coefficient $R^2 = 0.99$), the dimple diameter, D , could be estimated as follows:

$$D = 0.375 + 0.111V_{\text{HCl}} \quad (4)$$

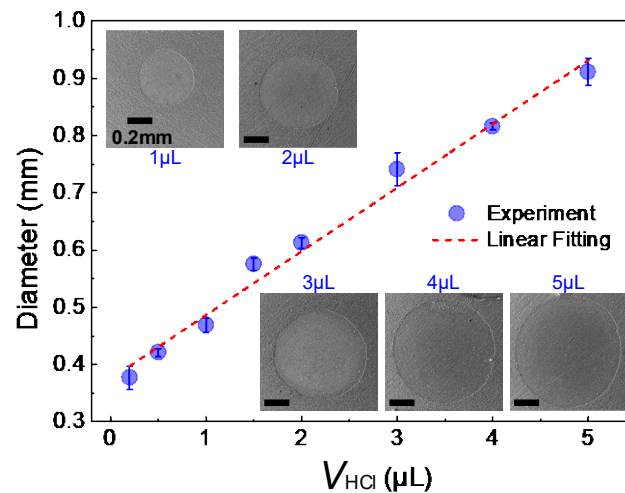


Figure 4. Relationship between the volume of deposited HCl droplet (V_{HCl}) and the diameter of the obtained dimple. Spots are the experimental values, while the dotted line is their linear fitting ($R^2 = 0.99$), and the inserted SEM images show the prepared dimples with different V_{HCl} .

Programmable liquid droplet manipulations, including controllable transfer and deposition, have been widely explored on wettability-patterned surfaces [55–58]. Here, we tested water droplet manipulations on the HCl etching-patterned hydrophilic/superhydrophobic surface. Figure 5 shows water droplet transfer by hydrophilic dimple-patterned superhydrophobic substrates. Figure 5a illustrates the schematic diagram of the pre-designed patterned surfaces, consisting of one hydrophilic dimple on each superhydrophobic substrate. As shown in the image in Figure 5b, a water droplet (5 μL) was initially pre-deposited at position A of the superhydrophobic surface; positions B and C were patterned with hydrophilic dimples with diameters of 0.62 mm and 0.81 mm, respectively. Figure 5c,d depict that an upward movement of the lower substrate enabled the contact between the droplet and dimple B, and then the droplet adhered to the upper substrate via dimple B when the lower plate was moved down. As can be seen in Figure 5e–h, when the hanging droplet came in contact with dimple C on the lower plate, it was grabbed by the dimple and then re-deposited onto the lower substrate, i.e., the droplet was transferred from position A to C. It could be observed that some liquid was left on the hydrophilic dimple B after the transfer, and its volume was estimated to be $\sim 0.03 \mu\text{L}$. Although the liquid deposition by the hydrophilic dimple was inevitable, the as-prepared patterned surface herein could be used for water droplet transfer after taking the dimple-diameter-dependent and quantifiable volume loss into consideration.

Figure 6 shows water droplets merging by using the as-prepared hydrophilic dimple-patterned superhydrophobic surfaces. As can be seen from Figure 6a, water droplets #1 (7.0 μL) and #2 (4.0 μL) were, respectively, deposited at position A (superhydrophobic area) and position B (a hydrophilic dimple with diameter of 0.81 mm); positions C and D on the upper plate were a hydrophilic dimple (diameter 0.62 mm) and a superhydrophobic area, respectively. Figure 6b–d show that after the two droplets came in contact with the upper plate at positions C and D, the subsequent downward movement of the lower plate enabled the capture of droplet #1 by the upper plate due to the high adhesion of dimple C, while droplet #2 remained at dimple B because the adhesion of position D, the original superhydrophobic surface, was extremely low. Then, horizontal and subsequently perpendicular movement of the lower substrate enabled the merging of droplets #1 and #2, resulting in the formation of a new droplet #(1 + 2) at dimple B, as depicted in Figure 6d–f. It has to be noted that a slight volume loss ($\sim 0.03 \mu\text{L}$) of droplet #1 was observed at position C during the merging, which should be taken into consideration in terms of quantitative droplet merging. Consequently, we could envision that the proposed chemical instability-

induced patterned superhydrophobic surfaces could be potentially used for droplet-based micro-reactors [59].

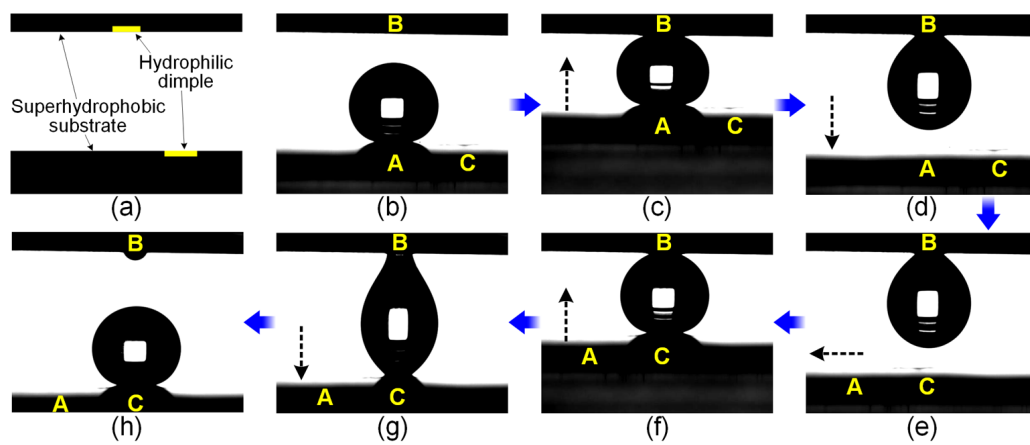


Figure 5. Water droplet transfer by hydrophilic dimple-patterned superhydrophobic substrates: (a) the schematic diagram of the employed substrates; (b–h) the image sequences showing the water droplet (5 μL) transfer from position A to C via dimple B; the black dotted arrows indicate the direction of movement of the lower substrate.

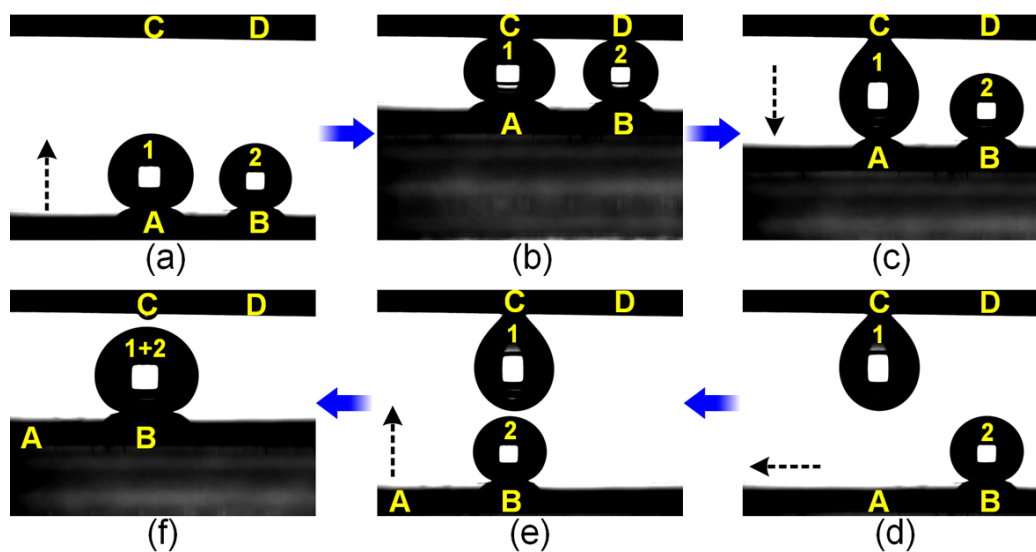


Figure 6. (a–f) Merging of water droplets 1 and 2 by hydrophilic dimple-patterned superhydrophobic substrates; the black dotted arrows indicate the moving direction of the lower substrate, A and B respectively indicate the superhydrophobic position and the hydrophilic dimple with diameter of 0.81 mm on the lower substrate, C and D represent the hydrophilic dimple with diameter of 0.62 mm and the superhydrophobic area on the upper substrate, respectively.

The deposition of nanoliter-sized droplets is important in many chemical and biomedical droplet-based microfluidic applications, such as fluorescence detection [55] and high-throughput cell screening [60]. We show here the nanoliter water deposition by the as-prepared hydrophilic dimple-patterned superhydrophobic surface, which is schematically illustrated in Figure 7a. As can be seen in Figure 7b, a water droplet (1.5 μL) attached to a needle was initially positioned on the superhydrophobic area of the patterned surface. When the substrate was horizontally moved with a velocity of ~ 0.6 mm/s, the droplet remained quasi-spherical in shape until it adhered to the dimple. Afterwards, the droplet gradually deformed and broke, leaving a tiny droplet deposited on the dimple. According to the schematic diagram in Figure 7c, the deposited water could be roughly considered as a spherical crown intercepted

from a sphere with radius of R to estimate its volume. The intercepted area's diameter (d) and height (h) of the spherical crown could be experimentally measured from the recorded images. According to the Pythagorean theorem, we know that:

$$x^2 + y^2 = R^2 \quad (5)$$

$$(R - h)^2 + (d/2)^2 = R^2 \quad (6)$$

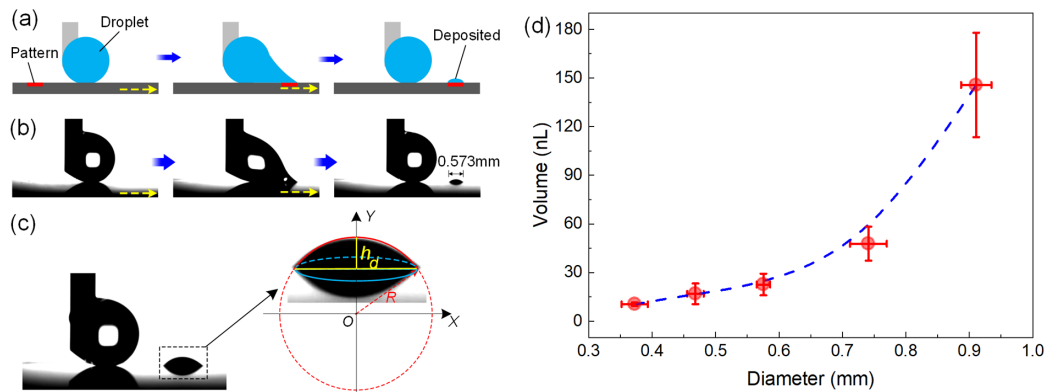


Figure 7. Nanoliter water deposition on hydrophilic dimple-patterned superhydrophobic substrates: (a) the schematic diagram and (b) image sequences showing a nanoliter water deposition process; the yellow arrows indicate the direction of movement of the substrate; (c) the schematic diagram of volume estimation for the deposited water; (d) the relationship between the diameter of hydrophilic dimple and the volume of deposited water droplet.

The volume of the deposited water, V_d , can be described as:

$$V_d = \int_{R-h}^R \pi x^2 dy \quad (7)$$

According to Equations (5)–(7), the volume of the deposited water can be expressed as:

$$V_d = \frac{\pi h(3d^2 + 4h^2)}{24} \quad (8)$$

According to Equation (8), the deposited water droplet in Figure 7b was calculated to be ~20 nL. Then, we prepared hydrophilic dimples with different diameters by using HCl droplets with varying volumes (Figure 4) and studied the influence of the dimple diameter on the volume of the deposited droplet. As shown in Figure 7d, the volume of the deposited droplet increased with the growth in dimple diameter within the examined regime, and a volume as low as 10.5 ± 1.1 nL could be deposited on the dimple with a diameter of 0.37 ± 0.02 mm. Besides droplet-based microfluidic applications, quantifiable droplet deposition can also be used to estimate the liquid loss during droplet transfer and merging, as depicted in Figures 5 and 6.

4. Conclusions

In summary, we reported a simple method to create hydrophilic patterns on a superhydrophobic Cu surface by using HCl solution-triggered chemical instability. A 2.5 min HCl exposure led to the etching of surface micro/nano structures and partial removal of the FAS molecular layers, enabling the treated superhydrophobic area to be hydrophilic. Based on this HCl-induced chemical instability, we prepared hydrophilic dimples with diameters of 0.38–0.91 mm by depositing HCl droplets with volumes of 0.2–5.0 μ L on the superhydrophobic surfaces. Typical applications, such as controlled droplet transfer, merging, and nanoliter droplet deposition, have been demonstrated on the hydrophilic dimple-patterned superhydrophobic surface. These results demonstrated the feasibility of creating wetta-

bility patterns on superhydrophobic surfaces by using their chemical instability towards corrosive solutions, which could enrich the fabrication methods of liquid-repellent surfaces with patterned wettability and promote their applications in droplet manipulation.

Author Contributions: Conceptualization, T.C. and F.C.; methodology, T.C. and F.C.; validation, T.C. and F.C.; formal analysis, T.C.; investigation, T.C.; resources, F.C.; data curation, F.C.; writing—original draft preparation, T.C.; writing—review and editing, F.C.; visualization, T.C. and F.C.; supervision, F.C.; project administration, F.C.; funding acquisition, F.C. All authors have read and agreed to the published version of the manuscript.

Funding: This research was funded by the National Natural Science Foundation of China, grant number 52105477.

Data Availability Statement: The data presented in this study are available on request from the corresponding author. The data are not publicly available due to a confidentiality request.

Conflicts of Interest: The authors declare no conflicts of interest.

References

1. Wang, D.; Sun, Q.; Hokkanen, M.J.; Zhang, C.; Lin, F.Y.; Liu, Q.; Zhu, S.P.; Zhou, T.; Chang, Q.; He, B.; et al. Design of robust superhydrophobic surfaces. *Nature* **2020**, *582*, 55–59. [[CrossRef](#)] [[PubMed](#)]
2. Su, W.; Lu, X.; Shu, Y.; Liu, X.; Gao, W.; Yao, J.; Niu, Z.; Xie, Y. Robust, Superhydrophobic Aluminum Fins with Excellent Mechanical Durability and Self-Cleaning Ability. *Micromachines* **2023**, *14*, 704. [[CrossRef](#)] [[PubMed](#)]
3. Xu, T.; Xu, L.P.; Zhang, X.; Wang, S. Bioinspired superwetable micropatterns for biosensing. *Chem. Soc. Rev.* **2019**, *48*, 3153–3165. [[CrossRef](#)] [[PubMed](#)]
4. Wang, L.; Wu, Y.; Li, G.; Xu, H.; Gao, J.; Zhang, Q. Superhydrophobic n-octadecylsiloxane (PODS)-functionalized PDA-PEI film as efficient water-resistant sensor for ppb-level hexanal detection. *Chem. Eng. J.* **2020**, *399*, 125755. [[CrossRef](#)]
5. Song, J.; Cheng, W.; Nie, M.; He, X.; Nam, W.; Cheng, J.; Zhou, W. Partial Leidenfrost Evaporation-Assisted Ultrasensitive Surface-Enhanced Raman Spectroscopy in a Janus Water Droplet on Hierarchical Plasmonic Micro-/Nanostructures. *ACS Nano* **2020**, *14*, 9521–9531. [[CrossRef](#)] [[PubMed](#)]
6. Li, H.; Yang, Q.; Hou, J.; Li, Y.; Li, M.; Song, Y. Bioinspired Micropatterned Superhydrophilic Au-Areoles for Surface-Enhanced Raman Scattering (SERS) Trace Detection. *Adv. Funct. Mater.* **2018**, *28*, 1800448. [[CrossRef](#)]
7. Zhao, Z.; Qin, S.; Wang, D.; Pu, Y.; Wang, J.-X.; Saczek, J.; Harvey, A.; Ling, C.; Wang, S.; Chen, J.-F. Multi-stimuli-responsive liquid marbles stabilized by superhydrophobic luminescent carbon dots for miniature reactors. *Chem. Eng. J.* **2020**, *391*, 123478. [[CrossRef](#)]
8. Yu, C.; Zhu, X.; Cao, M.; Yu, C.; Li, K.; Jiang, L. Superhydrophobic helix: Controllable and directional bubble transport in an aqueous environment. *J. Mater. Chem. A* **2016**, *4*, 16865–16870. [[CrossRef](#)]
9. Wang, X.; Bai, H.; Yang, J.; Li, Z.; Wu, Y.; Yu, C.; Jiang, L.; Cao, M. Designing Flexible but Tough Slippery Track for Underwater Gas Manipulation. *Small* **2021**, *17*, 2007803. [[CrossRef](#)]
10. Ma, H.; Cao, M.; Zhang, C.; Bei, Z.; Li, K.; Yu, C.; Jiang, L. Directional and Continuous Transport of Gas Bubbles on Superaerophilic Geometry-Gradient Surfaces in Aqueous Environments. *Adv. Funct. Mater.* **2018**, *28*, 1705091. [[CrossRef](#)]
11. Long, Z.; Zhao, Y.; Zhang, C.; Zhang, Y.; Yu, C.; Wu, Y.; Ma, J.; Cao, M.; Jiang, L. A multi-bioinspired dual-gradient electrode for microbubble manipulation toward controllable water splitting. *Adv. Mater.* **2020**, *32*, 1908099. [[CrossRef](#)] [[PubMed](#)]
12. Li, Q.; Guo, Z.G. Fundamentals of icing and common strategies for designing biomimetic anti-icing surfaces. *J. Mater. Chem. A* **2018**, *6*, 13549–13581. [[CrossRef](#)]
13. Vercillo, V.; Tonnicchia, S.; Romano, J.-M.; García-Girón, A.; Aguilar-Morales, A.I.; Alamri, S.; Dimov, S.S.; Kunze, T.; Lasagni, A.F.; Bonaccorso, E. Design Rules for Laser-Treated Icephobic Metallic Surfaces for Aeronautic Applications. *Adv. Funct. Mater.* **2020**, *30*, 1910268. [[CrossRef](#)]
14. Zhang, L.; Chu, X.; Tian, F.; Xu, Y.; Hu, H. Bio-Inspired Hierarchical Micro-/Nanostructures for Anti-Icing Solely Fabricated by Metal-Assisted Chemical Etching. *Micromachines* **2022**, *13*, 1077. [[CrossRef](#)] [[PubMed](#)]
15. Li, Z.; Wang, X.; Bai, H.; Cao, M. Advances in Bioinspired Superhydrophobic Surfaces Made from Silicones: Fabrication and Application. *Polymers* **2023**, *15*, 543. [[CrossRef](#)] [[PubMed](#)]
16. Wu, S.; Du, Y.; Alsaid, Y.; Wu, D.; Hua, M.; Yan, Y.; Yao, B.; Ma, Y.; Zhu, X.; He, X. Superhydrophobic photothermal icephobic surfaces based on candle soot. *Proc. Natl. Acad. Sci. USA* **2020**, *117*, 11240–11246. [[CrossRef](#)] [[PubMed](#)]
17. Chen, F.; Lu, Y.; Liu, X.; Song, J.; He, G.; Tiwari, M.K.; Carmalt, C.J.; Parkin, I.P. Table salt as a template to prepare reusable porous PVDF–MWCNT foam for separation of immiscible oils/organic solvents and corrosive aqueous solutions. *Adv. Funct. Mater.* **2017**, *41*, 1702926. [[CrossRef](#)]
18. Xia, L.; Chen, F.; Cai, Z.; Chao, J.; Tian, Y.; Zhang, D. Magnet-assisted selective oil removal from water in non-open channel and continuous oil spills clean-up. *Sep. Purif. Technol.* **2022**, *282*, 120119. [[CrossRef](#)]

19. Liu, H.; Zhang, Z.; Wu, C.; Su, K.; Kan, X. Biomimetic Superhydrophobic Materials through 3D Printing: Progress and Challenges. *Micromachines* **2023**, *14*, 1216. [[CrossRef](#)]
20. Zhu, Z.; Li, J.; Peng, H.; Liu, D. Nature-Inspired Structures Applied in Heat Transfer Enhancement and Drag Reduction. *Micromachines* **2021**, *12*, 656. [[CrossRef](#)]
21. Cho, H.J.; Preston, D.J.; Zhu, Y.; Wang, E.N. Nanoengineered materials for liquid-vapour phase-change heat transfer. *Nat. Rev. Mater.* **2016**, *2*, 16092. [[CrossRef](#)]
22. Miljkovic, N.; Wang, E.N. Condensation heat transfer on superhydrophobic surfaces. *MRS Bull.* **2013**, *38*, 397–406. [[CrossRef](#)]
23. Feng, J.; Chen, F.; Chao, J.; Cai, Z.; Liu, T.; Zhang, D.; Tian, Y. Anti-corrosion property of superhydrophobic copper mesh with one-step self-assembled perfluorothiolate monolayers. *Surf. Interface Anal.* **2022**, *54*, 1087–1097. [[CrossRef](#)]
24. Zhang, L.; Tan, Z.; Zhang, C.; Tang, J.; Yao, C.; You, X.; Hao, B. Research on Metal Corrosion Resistant Bioinspired Special Wetting Surface Based on Laser Texturing Technology: A Review. *Micromachines* **2022**, *13*, 1431. [[CrossRef](#)] [[PubMed](#)]
25. Zhang, D.; Wu, G.; Li, H.; Cui, Y.; Zhang, Y. Superamphiphobic surfaces with robust self-cleaning, abrasion resistance and anti-corrosion. *Chem. Eng. J.* **2021**, *406*, 126753. [[CrossRef](#)]
26. Tian, X.L.; Verho, T.; Ras, R.H.A. Moving superhydrophobic surfaces toward real-world applications. *Science* **2016**, *352*, 142–143. [[CrossRef](#)] [[PubMed](#)]
27. Zhang, W.; Wang, D.; Sun, Z.; Song, J.; Deng, X. Robust superhydrophobicity: Mechanisms and strategies. *Chem. Soc. Rev.* **2021**, *50*, 4031–4061. [[CrossRef](#)]
28. Chen, F.; Wang, Y.; Tian, Y.; Zhang, D.; Song, J.; Crick, C.R.; Carmalt, C.J.; Parkin, I.P.; Lu, Y. Robust and durable liquid-repellent surfaces. *Chem. Soc. Rev.* **2022**, *51*, 8476–8583. [[CrossRef](#)]
29. Pan, S.; Kota, A.K.; Mabry, J.M.; Tuteja, A. Superomniphobic surfaces for effective chemical shielding. *J. Am. Chem. Soc.* **2013**, *135*, 578–581. [[CrossRef](#)]
30. Wei, D.; Wang, J.; Liu, Y.; Wang, D.; Li, S.; Wang, H. Controllable superhydrophobic surfaces with tunable adhesion on Mg alloys by a simple etching method and its corrosion inhibition performance. *Chem. Eng. J.* **2021**, *404*, 126444. [[CrossRef](#)]
31. Li, Y.; Zhang, X.G.; Cui, Y.X.; Wang, H.Y.; Wang, J.X. Anti-corrosion enhancement of superhydrophobic coating utilizing oxygen vacancy modified potassium titanate whisker. *Chem. Eng. J.* **2019**, *374*, 1326–1336. [[CrossRef](#)]
32. Chen, F.; Xu, W.; Lu, Y.; Song, J.; Huang, S.; Wang, L.; Parkin, I.P.; Liu, X. Hydrophilic patterning of superhydrophobic surfaces by atmospheric-pressure plasma jet. *Micro Nano Lett.* **2015**, *10*, 105–108. [[CrossRef](#)]
33. Li, S.; Scheiger, J.M.; Wang, Z.; Dong, Z.; Welle, A.; Trouillet, V.; Levkin, P.A. Substrate-Independent and Re-Writable Surface Patterning by Combining Polydopamine Coatings, Silanization, and Thiol-Ene Reaction. *Adv. Funct. Mater.* **2021**, *31*, 2107716. [[CrossRef](#)]
34. Das, A.; Deka, J.; Raidongia, K.; Manna, U. Robust and Self-Healable Bulk-Superhydrophobic Polymeric Coating. *Chem. Mater.* **2017**, *29*, 8720–8728. [[CrossRef](#)]
35. Maji, K.; Das, A.; Dhar, M.; Manna, U. Synergistic chemical patterns on a hydrophilic slippery liquid infused porous surface (SLIPS) for water harvesting applications. *J. Mater. Chem. A* **2020**, *8*, 25040. [[CrossRef](#)]
36. Bai, H.; Wang, L.; Ju, J.; Sun, R.; Zheng, Y.; Jiang, L. Efficient water collection on integrative bioinspired surfaces with star-shaped wettability patterns. *Adv. Mater.* **2014**, *26*, 5025–5030. [[CrossRef](#)] [[PubMed](#)]
37. Ghosh, A.; Ganguly, R.; Schutzius, T.M.; Megaridis, C.M. Wettability patterning for high-rate, pumpless fluid transport on open, non-planar microfluidic platforms. *Lab Chip* **2014**, *14*, 1538–1550. [[CrossRef](#)]
38. Xu, T.; Shi, W.; Huang, J.; Song, Y.; Zhang, F.; Xu, L.-P.; Zhang, X.; Wang, S. Superwetable Microchips as a Platform toward Microgravity Biosensing. *ACS Nano* **2017**, *11*, 621–626. [[CrossRef](#)]
39. Huang, S.; Song, J.; Lu, Y.; Chen, F.; Zheng, H.; Yang, X.; Liu, X.; Sun, J.; Carmalt, C.J.; Parkin, I.P.; et al. Underwater Spontaneous Pumpless Transportation of Nonpolar Organic Liquids on Extreme Wettability Patterns. *ACS Appl. Mater. Interfaces* **2016**, *8*, 2942–2949. [[CrossRef](#)]
40. Liu, J.; Song, J.; Wang, G.; Chen, F.; Liu, S.; Yang, X.; Sun, J.; Zheng, H.; Huang, L.; Jin, Z.; et al. Maskless hydrophilic patterning of the superhydrophobic aluminum surface by an atmospheric pressure microplasma jet for water adhesion controlling. *ACS Appl. Mater. Interfaces* **2018**, *10*, 7497–7503. [[CrossRef](#)]
41. Liu, N.; Cao, Y.; Lin, X.; Chen, Y.; Feng, L.; Wei, Y. A Facile Solvent-Manipulated Mesh for Reversible Oil/Water Separation. *ACS Appl. Mater. Interfaces* **2014**, *6*, 12821–12826. [[CrossRef](#)] [[PubMed](#)]
42. Yang, C.; Wang, M.; Yang, Z.; Zhang, D.; Tian, Y.; Jing, X.; Liu, X. Investigation of Effects of Acid, Alkali, and Salt Solutions on Fluorinated Superhydrophobic Surfaces. *Langmuir* **2019**, *35*, 17027–17036. [[CrossRef](#)] [[PubMed](#)]
43. Dang, Z.; Liu, L.; Li, Y.; Xiang, Y.; Guo, G. In Situ and Ex Situ pH-Responsive Coatings with Switchable Wettability for Controllable Oil/Water Separation. *ACS Appl. Mater. Interfaces* **2016**, *8*, 31281–31288. [[CrossRef](#)] [[PubMed](#)]
44. Zeng, X.; Yang, K.; Huang, C.; Yang, K.; Xu, S.; Wang, L.; Pi, P.; Wen, X. Novel pH-Responsive Smart Fabric: From Switchable Wettability to Controllable On-Demand Oil/Water Separation. *ACS Sustain. Chem. Eng.* **2019**, *7*, 368–376. [[CrossRef](#)]
45. Huang, X.; Sun, Y.; Soh, S. Stimuli-Responsive Surfaces for Tunable and Reversible Control of Wettability. *Adv. Mater.* **2015**, *27*, 4062–4068. [[CrossRef](#)] [[PubMed](#)]
46. Chen, X.; Kong, L.; Dong, D.; Yang, G.; Yu, L.; Chen, J.; Zhang, P. Fabrication of Functionalized Copper Compound Hierarchical Structure with Bionic Superhydrophobic Properties. *J. Phys. Chem. C* **2009**, *113*, 5396–5401. [[CrossRef](#)]

47. Liu, Z.; Wang, H.; Zhang, X.; Wang, C.; Lv, C.; Zhu, Y. Durable and self-healing superhydrophobic surface with bistratal gas layers prepared by electrospinning and hydrothermal processes. *Chem. Eng. J.* **2017**, *326*, 578–586. [[CrossRef](#)]
48. Zhou, B.; Wu, Y.; Zheng, H. Investigation of Electrochemical Assisted Deposition of Sol-Gel Silica Films for Long-Lasting Superhydrophobicity. *Materials* **2023**, *16*, 1417. [[CrossRef](#)]
49. Lan, L.; Wang, H.; Zhu, L.; Di, Y.; Kang, J.; Qiu, J. Preparation and Wetting Mechanism of Laser-Etched Composite Self-Assembled 1H,1H,2H,2H-Perfluorodecyltriethoxysilane Superhydrophobic Surface Coating. *Phys. Status Solidi A* **2022**, *219*, 2100568. [[CrossRef](#)]
50. Zhai, N.; Fan, L.; Li, L.; Zhang, J. Durable superamphiphobic coatings repelling both cool and hot liquids based on carbon nanotubes. *J. Colloid Interface Sci.* **2017**, *505*, 622–630. [[CrossRef](#)]
51. Guo, Y.; Wu, H.; Li, Y.; Jiang, C.; Wang, Q.; Wang, T. Facile fabrication of superhydrophobic Cu(OH)₂ nanorod and CuO nanosheet arrays on copper surface. *J. Nanosci. Nanotechnol.* **2012**, *12*, 1952–1956. [[CrossRef](#)] [[PubMed](#)]
52. Çakır, O. Review of Etchants for Copper and Its Alloys in Wet Etching Processes. *Key Eng. Mater.* **2008**, *364–366*, 460–465.
53. Matsumoto, K.; Arai, H.; Taniguchi, S.; Kikuchi, A. Etching rate of copper by CuCl₂-HCl solution. *Trans. Jpn. Inst. Electron. Packag.* **2002**, *5*, 35–41. [[CrossRef](#)]
54. Cai, Z.; Chen, F.; Tian, Y.; Zhang, D.; Lian, Z.; Cao, M. Programmable droplet transport on multi-bioinspired slippery surface with tridirectionally anisotropic wettability. *Chem. Eng. J.* **2022**, *449*, 137831. [[CrossRef](#)]
55. Bachus, K.J.; Mats, L.; Choi, H.W.; Gibson, G.T.; Oleschuk, R.D. Fabrication of Patterned Superhydrophobic/Hydrophilic Substrates by Laser Micromachining for Small Volume Deposition and Droplet-Based Fluorescence. *ACS Appl. Mater. Interfaces* **2017**, *9*, 7629–7636. [[CrossRef](#)] [[PubMed](#)]
56. Xu, C.; Feng, R.; Song, F.; Wu, J.-M.; Luo, Y.-Q.; Wang, X.-L.; Wang, Y.-Z. Continuous and controlled directional water transportation on a hydrophobic/superhydrophobic patterned surface. *Chem. Eng. J.* **2018**, *352*, 722–729. [[CrossRef](#)]
57. Malinowski, R.; Parkin, I.P.; Volpe, G. Advances towards programmable droplet transport on solid surfaces and its applications. *Chem. Soc. Rev.* **2020**, *49*, 7879–7892. [[CrossRef](#)] [[PubMed](#)]
58. Shu, C.; Su, Q.; Li, M.; Wang, Z.; Yin, S.; Huang, S. Fabrication of extreme wettability surface for controllable droplet manipulation over a wide temperature range. *Int. J. Extrem. Manuf.* **2022**, *4*, 045103. [[CrossRef](#)]
59. Sun, L.; Bian, F.; Wang, Y.; Wang, Y.; Zhang, X.; Zhao, Y. Bioinspired programmable wettability arrays for droplets manipulation. *Proc. Natl. Acad. Sci. USA* **2020**, *117*, 4527–4532. [[CrossRef](#)]
60. Tronser, T.; Popova, A.A.; Jaggy, M.; Bastmeyer, M.; Levkin, P.A. Droplet Microarray Based on Patterned Superhydrophobic Surfaces Prevents Stem Cell Differentiation and Enables High-Throughput Stem Cell Screening. *Adv. Healthcare Mater.* **2017**, *6*, 1700622. [[CrossRef](#)]

Disclaimer/Publisher’s Note: The statements, opinions and data contained in all publications are solely those of the individual author(s) and contributor(s) and not of MDPI and/or the editor(s). MDPI and/or the editor(s) disclaim responsibility for any injury to people or property resulting from any ideas, methods, instructions or products referred to in the content.